Available online at www.sciencedirect.com
ScienceDirect
Superlattices and Microstructures 40 (2006) 289–294
Superlattices and Microstructures
www.elsevier.com/locate/superlattices

Correlation between structural and electrical properties of InN thin films prepared by molecular beam epitaxy

V. Lebedev[a,*], F.M. Morales[b], V. Cimalla[a], J.G. Lozano[b], D. González[b], M. Himmerlich[a], S. Krischok[a], J.A. Schaefer[a], O. Ambacher[a]

[a] *Institute of Micro- and Nanotechnologies, Technical University Ilmenau, D-98684 Ilmenau, Germany*
[b] *Dpto. de Ciencia de los Materiales e Ingeniería Metalúrgica y Química Inorgánica, Facultad de Ciencias, Universidad de Cádiz, 11510-Puerto Real-Cádiz, Spain*

Received 5 May 2006; received in revised form 5 July 2006; accepted 6 July 2006
Available online 17 August 2006

Abstract

The strain-relaxation phenomena and the formation of a dislocation network in 2*H*-InN epilayers during molecular beam epitaxy are reported. The proposed growth model emphasizes the dominant role of the coalescence process in the formation of a dislocation network in 2*H*-InN. Edge type threading dislocations and dislocations of mixed character have been found to be the dominating defects in wurtzite InN layers. It is demonstrated that these dislocations are active suppliers of electrons and an exponential decay of their density with the thickness implies a corresponding decay in the carrier density. Room temperature mobility in excess of 1500 $cm^2\ V^{-1}\ s^{-1}$ was obtained for ~800 nm thick InN layers with dislocation densities of $\sim 3 \times 10^9\ cm^{-2}$.

Keywords: InN; Epitaxy; Dislocations; Electron transport

1. Introduction

Recent studies of the narrow band gap InN semiconductor [1] show increasing interest in investigating its fundamental properties and evaluating potential applications. InN was predicted to have the lowest effective mass for electrons among all III-nitride semiconductors [2], resulting in high mobility and high saturation velocity suitable for high-frequency field effect transistors.

* Corresponding author. Tel.: +49 3677 693410; fax: +49 3677 693355.
E-mail address: vadim.lebedev@tu-ilmenau.de (V. Lebedev).

0749-6036/$ - see front matter © 2006 Elsevier Ltd. All rights reserved.
doi:10.1016/j.spmi.2006.07.006

Recently reported results reveal the promising applications of InN epilayers for chemical and biological sensors [3].

The most valuable problem of the InN heteroepitaxy is related to large lattice mismatches between the epilayer and any available substrate material. This raises the question of strain relaxation even for very thin epilayers, since the misfit dislocation densities in InN is initially $>10^{11}$ cm^{-2} [4]. In order to achieve high optical and electronic quality, misfit relaxation defects in InN should be avoided within the constituting layers. Up to date, a number of studies have been published on strain relief [4–7] and transport studies [8–11] of InN/Al$_x$Ga$_{1-x}$N heterostructures. However, detailed microstructure characterizations and a correlation with electrical properties have been rarely attempted. The purpose of this work is to study the strain relief, including the formation of dislocations, in (0001) InN/AlN heterostructures grown by plasma induced molecular beam epitaxy (PIMBE). Additionally the influence of structural growth defects on electron transport properties of undoped InN thin films will be discussed.

2. Experimental

The samples were grown in a Balzer's PIMBE system described elsewhere [12]. The growth process was monitored by digitized patterns of reflection high energy electron diffraction (RHEED). The (0001) AlN/Al_2O_3 epitaxial templates were overgrown *in situ* by 2*H*-InN epilayers (0.35–2.2 μm) at $T_{sub} \sim 380$ °C under stoichiometric (1:1) conditions to prevent a surface metal accumulation. The samples prepared for electrical characterization were processed by photolithography to form In point contacts with a spacing of 5 mm for Hall measurements. The contacts were annealed at 150 °C. Structural analysis was performed by high resolution X-ray diffraction (XRD) using a Bruker D8 diffractometer. The samples for cross-section and plan-view transmission electron microscopy (TEM) were prepared by mechanical thinning and ion-milling. The micrographs obtained in bright-field (BF) and dark-field (DF) modes by conventional two-beam (2B) conditions and high resolution TEM (HRTEM) were analyzed.

3. Results and discussion

After growth the chemical composition of the surface region was characterized by X-ray photoelectron spectroscopy (XPS) using monochromated Al K$_\alpha$ ($h\nu = 1486.7$ eV), radiation (Fig. 1) [13]. After loading, surface contaminations by oxygen and carbon due to exposure to ambient conditions are detected. Annealing at $T \sim 500$ K reduces most of the O contaminations and parts of the C impurities. Highly resolved spectra of the In$_3$d$_{5/2}$ and N1s states reveal that the *as loaded* sample is partially oxidized at the surface, which is evident from the existence of an In–O shoulder in the In3d$_{5/2}$ peak, whereas after annealing narrow peaks with a single component are observed. All binding energies are given with respect to the Fermi level of a silver reference sample. In both, the In3d and In4d (not shown) emission, no evidence for the existence of metallic indium is found.

X-ray diffraction (XRD) rocking curves at the (0002) InN reflection show a continuous decrease of the full width at half-maximum (FWHM) with increasing film thickness. The lowest FWHM of 0.277° was found at ∼1 μm indicating the continuous improvement of the InN layers up to this thickness and a change in the relaxation mechanism thereafter. Reciprocal space maps were taken around the symmetric (0002) and the asymmetric (20.5) reflections showing that InN layers of ∼1 μm thick have only a small residual stress <0.1%. The results agree very well with the previously [7] performed analysis of epitaxial InN samples grown at Cornell University.

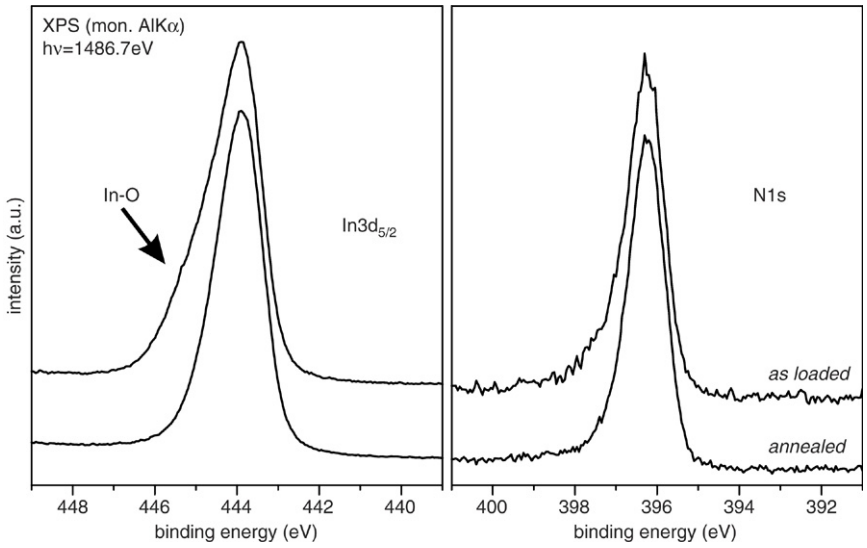

Fig. 1. X-ray photoelectron spectra of the InN surface before and after annealing. Shown are the $In3d_{5/2}$ and N1s core level spectra.

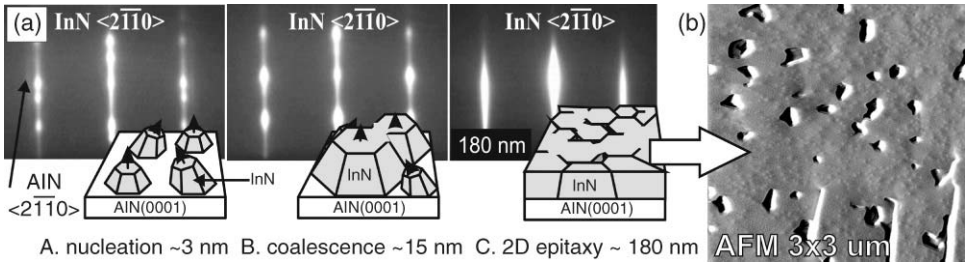

Fig. 2. (a) $\langle 2\bar{1}\bar{1}0\rangle$ RHEED patterns and schematic representation of the growth of $2H$-InN on highly mismatched templates: (A) early formation of the slightly misoriented flat InN platelets with elastic relaxation at the edges, (B) partial coalescence of the platelets, and (C) further growth and formation of a continuous layer. (b) AFM reveals a low roughness of ∼2 nm for a 2.2 μm InN surface.

The surface morphology was analysed by atomic force microscopy (AFM) using contact mode (Fig. 2(b)) revealing a typical rms roughness of ∼2 nm for ∼0.8 μm thick films.

The *in situ* RHEED observations allowed us to distinguish at least three different growth phases characteristic for any highly-mismatched heterosystem: (i) nucleation and subsequent growth of slightly misoriented $2H$-InN islands up to a thickness of ∼10–15 nm, (ii) a partial coalescence of the islands into a continuous film, and (iii) a long-term epitaxy followed by gradual improvements of the surface morphology (Fig. 2(a)).

In the $InN/Al_xGa_{1-x}N$ heterostructures, most of the lattice mismatch is accommodated by geometrical misfit dislocations (GMDs) [14], which are 60° dislocations with a Burgers' vector $\vec{b}$ and line parallel to $\langle 2\bar{1}10\rangle$ directions and lying on the (0001) basal plane. Statistical HRTEM analyses demonstrate an approximate ratio, $m{:}n$ [12], $InN\{01\bar{1}0\}{:}AlN\{01\bar{1}0\}$ of ∼57:64 resulting in a residual mismatch of $f = (n \times d_{AlN} - m \times d_{InN})/n \times d_{AlN} = -0.012$. A line density of dislocations near the AlN/InN heterointerface of $D_I \sim (4 \pm 0.5) \times 10^6$ cm^{-1} was extracted

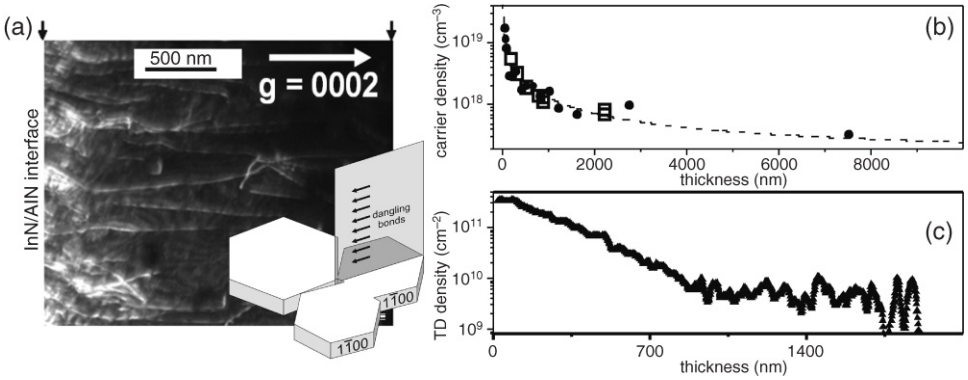

Fig. 3. (a) DF-TEM micrograph taken in 2B conditions using the 0002 reflection for pure screw $\vec{b} = \langle 0001 \rangle$ or mixed $\bar{b} = 1/3\langle 11\bar{2}3 \rangle$ TD detection. (Inset: A schematic view of the grain boundary TDs at the contact plane of the $2H$-InN islands.) (b) The Hall carrier density variations vs. thickness for a set of InN epilayers (open rectangles). The dashed line is an experimental data fit. Black circles represent the data published by Lu et al. (Ref. [8]). (c) TDs density vs. distance from the interface for a 2.2 μm thick InN epilayer derived from TEM.

from HRTEM images. During the coalescence (Fig. 2(a)-B), $2H$-InN domains come into contact forming a partially disordered phase [14,15]. The small in-plane misorientation, $\Delta\phi$, will give rise to a low-angle domain boundary, which consists of an array of dislocations with a spacing $D = |\vec{b}|/\tan(\Delta\phi)$. For $\vec{b} = 1/3\langle 11\bar{2}0 \rangle$ threading dislocations (TDs) and $\Delta\phi \sim 0.3°$, the dislocation density of $D_c \approx 7.7 \times 10^{10}$ cm^{-2} can be derived [16]. These $|\vec{b}| = 1/3\langle 11\bar{2}0 \rangle$ TDs are pure edge dislocations with no dislocation glide, produced by the domain structure of the film.

At a certain critical thickness [17], it may become possible that the strain energy is partially released by the generation of a new dislocation network of secondary misfit dislocations (SMDs) which glide to the island/substrate interface. The following slip systems: (a) $\{11\bar{2}2\}\langle 11\bar{2}3 \rangle$; and (b) $\{1\bar{1}01\}\langle 11\bar{2}3 \rangle$ were found to be the only possibility to form SMDs, to relieve the biaxial strain [6]. If we assume that each SMD could be related at least with one secondary $\bar{b} = 1/3\langle 11\bar{2}3 \rangle$ TD and its length is limited by the mosaic structure, a secondary planar TD density of $D_2 \sim 3.26 \times 10^{11}$ cm^{-2} can be deduced [16]. Finally, we can estimate the total density of TDs after the coalescence phase as follows: $D = D_c(\Im) + D_2(\Im) \sim 4 \times 10^{11}$ cm^{-2}. GMDs have not been taken into account so as they do not create dislocation lines propagating along the $\langle 0001 \rangle$ direction. The calculated total density of TDs fits well to the value obtained by the TEM observations; for example for dislocations with pure edge or mixed character at a thickness ~7.5 nm (experimental: 3×10^{11} cm^{-2}, extrapolated: 4×10^{11} cm^{-2}) (see Fig. 3).

Fig. 3(a) shows a DF-2B-TEM micrograph using the 0002 reflection of InN near the $[\bar{1}\bar{1}00]$ zone axis to display pure screw and mixed TDs. Similarly, TEM micrographs were taken in 2B conditions using the $11\bar{2}0$ reflection for pure edge $\bar{b} = 1/3\langle 11\bar{2}0 \rangle \vec{b} = 1/3\langle 11\bar{2}0 \rangle$ or mixed $\bar{b} = 1/3\langle 11\bar{2}3 \rangle$ TDs detection. From the intensity profiles of these images, as one can see in Fig. 3(c), the reduction in the dislocation density (N^{TD}) is seen to follow an exponential decay law up to a thickness of ~1 μm. The main mechanism of TDs annihilation in $2H$-InN is similar to those observed in $2H$-GaN [18] and $2H$-AlN [12].

Taking into account a full core TD model [19] for $\vec{b} = 1/3\langle 11\bar{2}0 \rangle$ and $\vec{b} = 1/3\langle 11\bar{2}3 \rangle$ TDs in $2H$-material as well as results of TD studies in GaN [9,19], a quantitative model of a bulk carrier generation in InN can be derived. In this model of carrier generation in

InN epilayers having thickness d have to include at least three independent components: $n_e = n_{\text{point}} + \frac{N_L}{d} + n_e^{\text{TD}}$ [cm^{-3}], where n_{point} is the background carrier density of $\sim 10^{17}$ cm^{-3}, which is a sum of intrinsic, impurity- and point-defect-generated carrier concentrations and $N_L \sim 2.5 \times 10^{13}$ cm^{-2} is the localized sheet carrier density near the InN surface [3,8,20]. The contribution of the TD-induced electrons (n_e^{TD}) into the total free carrier density as a function of the epilayer thickness can be estimated using an empirical formula: $n_e^{\text{TD}} = \frac{1}{d}\sum_{i=1}^{k} N_i^{\text{TD}}$ [cm^{-3}]. Here we assume that a non-complete ionization of atoms along an ideal dislocation line yields $\sim$1 electron per $\lambda \sim 2 \times c_{\text{InN}}$ of dislocation length and $k = d/\lambda$. A model fit is presented in Fig. 3(b) by the dashed line. Black circles representing the data published by Lu et al. [8] have been used as a reference. The fit of the data shows an excellent agreement for $\lambda \sim 1.1$ nm. Here, we have to point out that the assumption of the non-complete ionization of atoms along the dislocation line gives an uncertainty factor in the numerical estimations. Mixed character of the TDs also plays a role reducing the number of the defect-generated electrons. Finally, room temperature mobility in excess of 1500 cm^2 V^{-1} s^{-1} were obtained for $\sim$800 nm thick InN layers with dislocation densities of $\sim 3 \times 10^9$ cm^{-2}.

4. Conclusions

In conclusion, the proposed growth model emphasizes a determinant role of the residual strain relief and coalescence processes in the formation of $\vec{b} = 1/3\langle 11\bar{2}0\rangle$ TD network in $2H$-InN as revealed by RHEED, TEM and XRD measurements. It has been shown that the TD density decreases exponentially during film growth due to annihilation of the dislocations reaching $\sim$1–3 $\times 10^9$ cm^{-2} in $\sim$2.2 μm thick InN films. It is demonstrated that dislocations are active suppliers of electrons and the observed exponential decay of their density with the thickness implies the corresponding decay in the carrier density. Finally, cleanliness and quality of the grown samples were characterized via X-ray photoelectron spectroscopy.

Acknowledgements

This work was supported by the DFG grant AM105/1-1 (Germany) and CICYT project MAT2004-01234 (Spain). F.M.M. would like to thank the financial support under a Humboldt Research Fellowship SPA/1114640STP.

References

[1] V. Davydov, et al., Phys. Status Solidi b 229 (2002) R1; 230 (2002) R4.
[2] S.N. Mohammad, H. Morkoc, Prog. Quantum Electron. 20 (1996) 361.
[3] H. Lu, W.J. Schaff, L.F. Eastman, J. Appl. Phys. 96 (2004) 3577.
[4] E.B. Amalric, C. Adelmann, E. Sarigiannidou, J.L. Rouvière, G. Feuillet, E. Monroy, B. Daudin, J. Appl. Phys. 95 (2004) 1127.
[5] Y.F. Ng, Y.G. Cao, M.H. Xie, X.L. Wang, S.Y. Tong, Appl. Phys. Lett. 81 (2002) 3960.
[6] S. Srinivasan, L. Geng, R. Liu, F.A. Ponce, Y. Narukawa, S. Tanaka, Appl. Phys. Lett. 83 (2003) 5187.
[7] V. Cimalla, Ch. Förster, G. Kittler, I. Cimalla, R. Kosiba, G. Ecke, O. Ambacher, R. Goldhahn, S. Shokhovets, A. Georgakilas, H. Lu, W. Schaff, Phys. Status Solidi c 0 (2003) 2818.
[8] H. Lu, W. Schaff, L. Eastman, C.E. Stutz, Appl. Phys. Lett. 82 (2003) 1736;
H. Lu, W.J. Schaff, L.F. Eastman, J. Wu, W. Walukiewicz, D.C. Look, R.J. Molnar, MRS Symp. Proc. 743 (2003) L4.10.
[9] D.C. Look, H. Lu, W.J. Schaff, J. Jasinski, Z. Liliental-Weber, Appl. Phys. Lett. 80 (2002) 258.
[10] L.H. Dmowski, J.A. Plesiewicz, T. Suski, H. Lu, W. Schaff, M. Kurouchi, Y. Nanishi, L. Konczewicz, V. Cimalla, O. Ambacher, Appl. Phys. Lett. 86 (2005) 262105.

[11] E. Dimakis, E. Iliopoulos, K. Tsagaraki, Th. Kehagias, Ph. Komninou, A. Georgakilas, J. Appl. Phys. 97 (2005) 113520.
[12] V. Lebedev, F.M. Morales, H. Romanus, S. Krischok, G. Ecke, V. Cimalla, M. Himmerlich, T. Stauden, D. Cengher, O. Ambacher, J. Appl. Phys. 98 (2005) 093508.
[13] S. Krischok, V. Yanev, O. Balykov, M. Himmerlich, J.A. Schaefer, R. Kosiba, G. Ecke, I. Cimalla, V. Cimalla, O. Ambacher, H. Lu, W.J. Schaff, L.F. Eastman, Surf. Sci. 566–568 (2004) 849.
[14] X.J. Ning, F.R. Chien, P. Pirouz, J.W. Yang, M.A. Khan, J. Mater. Res. 11 (1996) 580.
[15] I. Akasaki, H. Amano, Y. Koide, K. Hiramatsu, N. Sawaki, J. Cryst. Growth 98 (1989) 209.
[16] A. Bourret, C. Adelmann, B. Daudin, J. Rouvière, G. Feuillet, G. Mula, Phys. Rev. B 63 (2001) 245307.
[17] F. Frank, J. van der Merwe, Proc. R. Soc. London 198 (1949) 205.
[18] S. Tanaka, M. Takeuchi, Y. Aoyagi, Japan. J. Appl. Phys., 2 39 (2000) L831.
[19] A.F. Wright, U. Grossner, Appl. Phys. Lett. 73 (1998) 2751.
[20] V. Cimalla, M. Niebelschütz, G. Ecke, V. Lebedev, O. Ambacher, M. Himmerlich, S. Krischok, J.A. Schaefer, H. Lu, W.J. Schaff, Phys. Status Solidi a 203 (2006) 59.